Effect of nitrogen limitation and soil processes on ~~mid~~ Holocene greening of the Sahara

Jooyeop Lee[1], Martin Claussen[2,3], Jeongwon Kim[1], Je-Woo Hong[4], In-Sun Song[5], and Jinkyu Hong[1]

[1]Ecosystem-Atmosphere Process Laboratory, Department of Atmospheric Sciences, Yonsei University, Seoul, Korea (Republic of)
[2]Max-Planck-Institut für Meteorologie, Hamburg, Germany
[3]Center for Earth System Research and Sustainability (CEN), Universität Hamburg, Germany
[4]Korea Adaptation Center for Climate Change, Korea Environment Institute, Sejong, Korea (Republic of)
[5]Mathematical Atmospheric Physics Lab, Department of Atmospheric Sciences, Yonsei University, Seoul, Korea (Republic of)

Correspondence to: Jinkyu Hong (jhong@yonsei.ac.kr)

Abstract. The so–called Green Sahara (GS), wet and vegetative Sahara region in the early to mid–Holocene, provides useful information on our climate simulation because it is a consequence of complex interaction between biophysical and climatic processes. It is still a challenge to simulate the GS in terms of vegetative extent and precipitation using the current climate models. This study attempts to simulate the 8,000 year ago Green Sahara by using the state–of–the–art earth system model CESM that incorporates the nitrogen cycle and the soil–~~albedo~~–precipitation ~~feedback~~feedbacks. Our study ~~focuses~~puts more emphasis on the impact of soil biophysical properties and soil nitrogen influenced by soil organic matter on the simulation of the GS. In this fully coupled simulations, vegetation interacts with changes in soil properties and soil organic matter by phenology, decomposition and allocation of carbon and nitrogen. With changes in the Earth's orbit and dust in the early to mid–Holocene, the model simulates increased precipitation in North Africa, but does not capture the extent of the GS. ~~Further~~Our analysis shows that the ~~mid~~ Holocene greening is simulated better if the amount of soil nitrogen and soil texture are properly modified ~~during the GS period~~for the humid and vegetative GS period. Soil biochemical and physical properties increase precipitation and vegetation cover in North Africa through their influence on photosynthesis and surface albedo and their consequent enhanced albedo– and evapotranspiration–precipitation feedbacks. Our findings suggest that future climate simulation needs to consider consequent changes in soil nitrogen and texture with changes in vegetation cover and density for proper climate simulations.

1. Introduction

Sahara is the largest subtropical desert on Earth, but it was wetter and had more vegetation than today during the early to mid–Holocene (~~MH~~EMH hereafter) (Holmes, 2008). In this Green Sahara (GS hereafter) period, the region was covered with various vegetation, inland rivers and mega–lakes (Pachur and Kröpelin, 1987; Jolly et al., 1998; Schuster et al., 2005; Quade

et al., 2018) up to 23° N of North Africa, unlike the current vegetation which only exists in regions below 15° N. The GS was sensitive to climate change with locally rapid transitions from a humid to a more arid state some 8,000 to 5,000 years ago (Shanahan et al., 2015). The GS and its transition to an arid state are the results of complex interactions of the orbital forcing

35 changes with the land–atmosphere interaction, and sea surface temperature (SST) variability (Claussen et al. 2017; Braconnot et al., 2019). Our futureFuture climate prediction ispredictions are made using Earth system models (ESMs), and recent progress in the development of ESMs made it possible to simulate and to assess the carbon–climate feedbacks. GS is a good platformexample to evaluate various feedback processes in ESMsthe state-of-the-art ESMs and to evaluate the model performance accordingly (Harrison et al., 2015; Pausata et al., 2020). In these respectsthis context, the GS period provides

40 unique and useful insights for our climate prediction in a changing climate.

Many modeling studies have been tried to simulate the GS and to understand the underlying mechanisms of the GS correctly. Early studies focused on the impacts of change in the Earth's orbit leading to higher summer solar insolation compared to the present (Kutzbach et al., 1981; Kutzbach and Street-Perrott, 1985). Further studies revealed that the following factors contributed to the amplification of the GS; the ocean–climate feedback (Kutzbach and Liu, 1997; Braconnot et al., 1999),

45 vegetation–climate feedback (Claussen, 1998; Claussen et al., 1999; Claussen et al., 2013; Rachmayani et al., 2015; Groner et al., 2018), soil–climate feedback (Kutzbach et al., 1996; Knorr et al., 2001; Levis et al., 2004; Knorr et al., 2006; Vamborg et al., 2011; Lu et al., 2018), inland water (Coe and Bonan, 1997; Krinner et al., 2012), and dust–climate feedback (Pausata et al., 2016; Gaetani et al., 2017). However, current state–of–the–art climate models still yield diverging results regarding the extent of the GS and the understanding of feedback processes (Claussen et al., 2017).

50 Recent progress in the development ofRecently, ESMs made it possiblebegan to simulate andcouple nitrogen (N hereafter) processes to assess the carbon–climate feedbacks. Particularly, cycle. The global carbon budget has been simulated more realistically with the recent inclusion of the nitrogen cycle in the ESM, global carbon budget has been better captured by its downregulation because of the N–limitation effect of terrestrial gross primary production (GPP) (Thornton et al., 2007; Castillo et al., 2012; Arora et al., 2020). Furthermore, vegetation However, impact of nitrogen limitation on the GS simulation has not

55 been extensively investigated as far as we know. It is also notable that soil in the GS led toincludes more simulatedorganic matter and humus compared to the current condition because vegetation leads to more organic matter in soils and therefore, thus affecting hydraulic, thermal, and radiative properties of soil. (e.g., Kutzbach et al., 1996; Levis et al., 2004; Lu et al., 2018). Lu et al. (2018) concluded that organic matter in soil texture changes likely played an important role in the GS dynamics, but their study was based on the offline land surface model only with changes in soil hydraulic and thermal properties. Although

60 and more studies need to be done to investigate impacts of the biophysical and biogeochemical changes in soil are important factors on the GS simulations, no previous studies investigated the GS in perspective of soil carbon and nitrogengreening in the framework of the fully coupled ESMs.

The present study aims at assessing the performance offocuses on better understanding of the ESM's simulation ability to simulate vegetation in the GS and its uncertainties by the representation of physical processes in the land surface model. We

65 investigate the impacts of nitrogen limitation and soil biophysical processes on the GS simulations using the Community Earth

System Model (CESM)~~,~~) version 1.2) (Hurrell et al., 2013~~) with interactive carbon–nitrogen cycle and dynamic vegetation~~ ~~parameterizations to simulate the mid-Holocene greening of the Sahara. We focus on the ability of the CESM to simulate~~). Based on a ~~Holocene~~series of the model simulations, we examine changes in the GS extension and its associated uncertainties by related ~~to soil~~factors of orbital forcing, nitrogen and carbon. ~~This enables us to improve our understanding of the model's~~ ~~simulation ability and the representation of physical processes in the CESM land surface model.~~ in soil, and soil texture.

2. Methods

2.1 Model description

The Community Earth System Model (CESM, version 1.2) with the Community Atmosphere Model version 4 (CAM4; Neale et al., 2013) and Community Land Model version 4 (CLM4; Oleson et al., 2010; Lawrence et al., 2011) is employed in this study. The CESM incorporates prognostic carbon–nitrogen (CN) equations and the dynamic vegetation model into the land surface model. The model simulates carbon dynamics such as productivity, phenology, decomposition and allocation with carbon and nitrogen fluxes at the ecosystem-atmosphere interface by the CN prognostic equations. This new CN parameterization makes a substantial difference in vegetation simulation by limiting gross primary production (GPP) with soil mineral nitrogen in the climate simulations particularly (Thornton et al., 2007; Castillo et al., 2012; Arora et al., 2020):

$$GPP = GPP_p \cdot \left(1 - \frac{CF_{excess}}{GPP_p}\right) \qquad (1)$$

~~where GPPp is~~ GPP becomes the potential GPP ~~from~~ (GPP_p) if there is no nitrogen limitation and nitrogen limitation is linked to soil organic matter in the ~~photosynthesis~~ model ~~and~~. Nitrogen limitation on GPP is expressed by CF_{excess} ~~is the excess of~~ ~~carbon fluxes (Eq. (1)). Appendix A lists the symbols used in this study. CFexcess is calculated as series of functions with soil~~ ~~nitrogen and carbon (Eq. (2)–(7)):~~

$$CF_{avail\_alloc} = GPP - MR \qquad (2)$$

$$N_{plant\_demand} = CF_{avail\_alloc} \cdot \frac{k_{n\_alloc}}{k_{c\_alloc}} - N_{retrans} \qquad (3)$$

$$N_{uptake} = \frac{N_{sminn}}{\Delta t} - NF_{immob} \qquad (4)$$

$$f_{pg} = \frac{N_{uptake}}{N_{plant\_demand}} \qquad (5)$$

which is decided by $CF_{alloc} = (N_{plant\_demand} \cdot f_{pg} + N_{retrans}) \cdot \frac{k_{c\_alloc}}{k_{n\_alloc}}$

$$\qquad (6)$$

~~$CF_{excess} - CF_{avail\_alloc} \cdot CF_{alloc}$~~ (7)

~~In this procedure,~~ soil mineral nitrogen ~~determines~~(N_{sminn}). N_{sminn} is a function of the conversion rate of soil organic nitrogen to mineral nitrogen ($NF_{soil4n \rightarrow sminn}$) and is affected by the amount of soil ~~nitrogen absorbed by the vegetation and~~ carbon ($soil4c$) ~~eventually regulates the first estimate of GPP to the smaller final GPP value (Eq. (1)), indicating the importance of the absolute amount of soil nitrogen and carbon when the nitrogen cycle is considered in the model.~~(Eq. (2) – (9)). It was reported that GPP in CESM version 1 was smaller than other CMIP6 models because of the larger nitrogen limitation effect. More details on the CN parameterization in the CLM can be found in Thornton et al. (2002), Thornton et al. (2009), and Kluzek (2012). ~~All~~The description of the ~~symbols and~~ variables used in this study ~~is~~including those in Equation 1 are listed in ~~Supplement~~Appendix A.

$$CF_{excess} = CF_{avail\_alloc} - CF_{alloc} \tag{2}$$

$$CF_{avail\_alloc} = GPP_p - MR \tag{3}$$

$$CF_{alloc} = \left(N_{plant\_demand} \cdot f_{pg} + N_{retrans}\right) \cdot \frac{k_{c\_alloc}}{k_{n\_alloc}} \tag{4}$$

$$f_{pg} = \frac{N_{uptake}}{N_{plant\_demand}} \tag{5}$$

$$N_{plant\_demand} = CF_{avail\_alloc} \cdot \frac{k_{n\_alloc}}{k_{c\_alloc}} - N_{retrans} \tag{6}$$

$$N_{uptake} = \frac{N_{sminn}}{\Delta t} - NF_{immob} \tag{7}$$

$$N_{sminn} = N_{sminn} + NF_{soil4n \rightarrow sminn} * dt \tag{8}$$

$$NF_{soil4n \rightarrow sminn} = \frac{soil4c * k_{decomp}}{dt * 10} \tag{9}$$

The albedo–precipitation feedback has been also considered to be one of the important aspects in the land–atmosphere interaction and should be clearly examined in the GS simulation (e.g., Charney, 1975; Cess, 1978; Bonfils et al., 2001; Houldcroft et al., 2009; Levine and Boos, 2017). Precipitation increases if surface albedo decreases because of more vegetation through the stratification of the atmosphere particularly in drylands. However, in the CMIP5 (Coupled Model Intercomparison Project 5) ~~MHEMH~~ simulations, ~~surface albedo~~ soil moisture is irrelevant to ~~soil moisture~~ surface albedo in most land surface models (LSMs) (e.g., Takata et al., 2003; Zeng, 2005; Houldcroft et al., 2009; Oleson et al, 2010; Watanabe et al., 2010; Vamborg et al., 2011). This study uses CLM4 for simulation of land surface processes. In the CLM4, surface albedo is~~, however,~~ parameterized as a function of soil moisture in the calculation of soil background albedo. In this parameterization, soil background albedo decreases with increases in soil moisture of the first soil layer as follows:

$$\alpha_{soil} = \alpha_{sat} + \Delta \le \alpha_{soil} \qquad (8)$$

$$\Delta = (0.11 - 0.40\theta_1) > 0 \begin{cases} 0.11 - 0.40\theta_1 & (\theta_1 \le 0.275) \\ 0 & (\theta_1 > 0.275) \end{cases}$$

$$(9)$$

In addition, the soil texture distribution is classified by sand and clay percentage and soil has 20 color classes from ~~low albedo (color class 20) to high albedo (color class 1).~~ the low to the high albedo. In the lowest albedo (darkest soil), dry (saturated) albedo is 0.08 (0.04) and 0.16 (0.08) in visible and NIR range, respectively. In the highest albedo (lightest soil), the dry (saturated) albedo is 0.36 (0.25) and 0.61 (0.50) in visible and NIR range, respectively. α_{sat} is equal to the albedo of the saturated soil.

2.2 Experimental design

For our CESM simulations of the GS, the horizontal resolution is 4°×5° in global scale with 26 vertical levels. The initial land surface data are made using CLM4 offline simulations for 600 years in the CN accelerated decomposition mode (Thornton and Rosenbloom, 2005), and then using 1200–year CLM4 simulations with the CNDV (Carbon–Nitrogen–Dynamic–Vegetation) with the atmospheric forcing data of 1948–1972 years based on Qian et al. (2006). The present (i.e., 0K) and ~~MH~~EMH (i.e., 8K) simulations are 500–year climate simulations using the pre–industrial and ~~MH~~EMH conditions, respectively (Table 1). The ~~MH~~EMH period is set to 8000 years ago (8K) in this study because 8K period was relatively greener than other periods (Jolly et al., 1998; Groner et al., 2018).

Additional sensitivity experiments using the ~~MH~~EMH conditions are conducted with different land states to examine the impacts of soil nitrogen, soil texture, and the mega lake on the GS simulation (Table 1). ~~In the 8KCN simulation, soil carbon and nitrogen are increased, and soil texture change to loam iss added to the 8KCN in the 8KCNS (Fig. 1).~~ Soil carbon and nitrogen are negligible in the current Sahara. To the best of our knowledge, there is no information on soil organic carbon and nitrogen in North Africa during the ~~MH~~EMH. It is reasonable to consider more soil carbon and nitrogen in the GS than in the present–day Sahara, because of their close coupling with biomass (Brooks, 2003; Wang et al., 2010; Yang et al., 2014). To consider the possibility of relatively larger soil carbon and nitrogen in the GS, ~~initial~~more soil carbon and nitrogen ~~in the vegetated area reported by~~are added with less sandy soil (i.e., loamier soil with more soil organic matter) in the 8KCN and 8KCNS experiments based on Jolly et al. (1998) to prescribe soil organic matter in the GS (i.e., 10–22° N, 345° W–40° E) ~~are prescribed~~ using nearby grassland grid values ~~in the 8KCN~~ (Fig. 1). In these sensitivity experiments, the feedbacks between vegetation and increased soil carbon and nitrogen evolve dynamically in the model through litter–fall and decomposition processes.

In all ~~MH~~EMH simulations, the Earth's orbital parameters and atmospheric CO_2 concentration are prescribed based on Berger (1978) with pre-industrial SST (Table 2), and atmospheric dust is reduced following Pausata et al. (2016) (Fig. 2). In

150 addition, the ~~Mega~~ Lake Mega–Chad is considered in our ~~MH~~EMH simulations by assigning 73% of the two grids near the Lake Chad region (14–18° N, 15° E) as lake area to consider the extensive Lake Chad in the ~~MH~~EMH (Leblanc et al., 2006; Quade et al., 2018). Our analysis focuses on three critical regions in North Africa around the border of the vegetation in our simulation: the North Africa of 20° N (solid boxed area in Fig. 3, NA hereafter), northern Sahara–Sahel region (dotted box area in Fig. 3, NSS hereafter), and Southern Sahara–Sahel region (dashed box area in Fig. 3, SSS hereafter). These regions are

155 selected as the analysis region because the SS region was sensitive to precipitation–land interaction (Kutzbach et al., 1996), and the NA region is closely related to the onset and progress of the African Monsoon (Levis et al., 2004).

3. Results and Discussion

3.1 Climate and vegetation simulation in the Green Sahara

~~Figure 3 shows the~~The 8K simulation shows typical climate patterns in the Sahara–Sahel (SS) region during the EMH and

160 there are substantial differences of surface climates between the 0K and 8K experiments in North Africa (~~8K-0K). The 8K simulation shows climate patterns in the Sahara-Sahel (SS) region during the MH.~~Fig. 3). The summer downward radiation at the top of the atmosphere increases by 6% in the SS region ~~than~~compared to the present because of the change in the orbital forcing and less amount of dust in the ~~MH~~EMH. This increase of solar radiation leads to an increase in surface shortwave radiation and net radiation by 30 and 21 W m^{-2}, respectively and subsequent temperature warming by 1.8° C in the NA region

165 in the 8K experiment (Fig. 3). ~~This~~The intensified land–sea thermal contrast ~~yield~~during the EMH makes spatial changes in precipitation and wind pattern over Holocene North Africa compared to the present climate.

~~However~~ Notably, the ~~increase~~increases in air temperature ~~is~~and shortwave radiation are not substantial in the ~~southern part of~~ SS region (less than 10% compared to the NA ~~area,~~region), because ~~of~~ the increase in precipitation and clouds with the northward migration of the monsoon ~~(Fig.~~ by the intensified land-sea thermal contrast (Fig. 3d). ~~In~~Indeed, the ~~8K experiment,~~

170 meridional wind in the 18° N region changed from northerly (~~-0~~-0.7 ms^{-1}) to southerly (0.3 ms^{-1}) in the ~~MH~~8K experiment (Fig. 3g, 3h), indicating a northward shift of the Intertropical Convergence Zone (ITCZ) (i.e., the convergence zone of the trade winds) to above 18° N. This ITCZ shift ~~made~~caused a favorable condition for a moister Sahara by transporting more moisture and subsequent more precipitation ~~in both of~~to the ~~NSS and SSS~~SS region (Chikira et al., 2006; Larrasoaña et al., 2013). Compared to the pre–industrial simulation (i.e., 0K), summer precipitation in the ~~MH~~EMH simulation (i.e., 8K)

175 increases by 18% (from 4.0 to 4.7 mm day^{-1}) and 15% (from 2.5 to 2.9 mm day^{-1}) in the SSS and NSS region, respectively (Fig. 3e, 3f).

The pre–industrial simulation captures the observed spatial extent of the current Sahara based on MODIS (Moderate Resolution Imaging Spectroradiometer) land surface data (Fig. 4a) (Broxton et al., 2014). ~~However~~Importantly, the model does not simulate increased vegetation fraction, despite the increased precipitation over the SS region during the ~~MH~~EMH

180 (Fig. 4b). Reconstruction of vegetation based on the pollen records reveals that grass and trees expanded up to 26° N and 20°

N over North Africa during the GS period, respectively (Hely et al., 2014; Hopcroft et al., 2017). Also, leaf wax data indicatedindicates that the GS extended more upas far north toas 31° N (Tierney et al., 2017). In contrast to the proxy data, vegetation fraction and GPP shows negligible changes in North Africa and even a decrease in western Africa and the southern border of the current Sahara in the 8K simulation (Fig. 4b, 4e). It is notable that Lake Mega–Chad did not make substantial changes in simulated summer precipitation northward movement of the 200 and 412 mm year^{-1} precipitation isohyet for 20 % grassland cover, which is similar to Contoux et al. (2013) (Fig. S1, S2).

Hopcroft et al. (2017) attributed such underestimation of the GS to excessive precipitation requirement for vegetation growth in the model (Table 3). Indeed, ourOur investigation also shows that the minimum amount of precipitation for vegetation growth is 577 mm year^{-1} in the 8K experiment. Notably, and this precipitation threshold for vegetation is larger than the observation value of 281 mm year^{-1} and the values of other land surface models reported in (Hopcroft et al. (., 2017). This larger threshold indicates that our model has relatively little vegetation cover with respect to the same amount of precipitation. However, this uncertainty and is not fully understood yet in the model has not been clearly discussed in previous studies.ESM (Hopcroft et al., 2017). Our investigation reveals that this excess water requirement by vegetation growth is partially related to becomes smaller with improved water use efficiency (WUE) with proper assignment of soil nitrogenorganic matter and soil texture, which is discussed in the next section. It is also notable that Mega–Lake Chad does not make substantial changes in simulated summer precipitation northward movement of the 200 and 412 mm year^{-1} precipitation isohyet for 20 % grassland cover, which is similar to Contoux et al. (2013) (Fig. S1, S2).

3.2 Impact of soil nitrogen on the Green Sahara simulation

The 8KCN experiment is designed to study the effect of an increase in soil nitrogen on the GS. Theby vegetation on the GS and simulates typical surface climate patterns during the EMH (not shown here). Importantly, the 8KCN simulation reproduces larger precipitation and vegetative areas with an increase in GPP in the SS region, compared to the 8K experiment (Fig. 4). TheVegetation fraction increases about twice in the SS region (21 % and 8 % in the SSS and NSS regions, respectively) in the 8KCN experiment (Table 4). The 8KCN experiment also shows 2 times larger vegetation fraction than the 8K experiment around the boundary of precipitation changes between the present and EMH (about 18° N). Particularly, the 8KCN experiment shows 3.3 and 5.3 times larger GPP in the NSS and SSS regions, respectively, compared to the 8K experiment (Table 5). Consequently, the precipitation threshold for vegetation decreases to 412 mm year^{-1} in the 8KCN from 577 mm year^{-1} in the 8K experiment (Fig. 5). Consequentlytogether with increased WUE values (Fig. 5 and 6). With this increase in vegetation fraction, the desert–grassland boundary moves one grid box northward in the 8KCN simulation compared to the 8K experiment (Fig. 4i). Vegetation fraction increases about twice in the SS region (23 % and 13 % in the SSS and NSS regions, respectively) in the 8KCN experiment. Particularly, the 8KCN experiment shows 3 times larger vegetation fraction than the 8K experiment around the boundary of precipitation changes between the present and MH (about 18° N). With this increase in vegetation

fraction, the 8KCN experiment shows 3.3 and 5.3 times larger GPP in the NSS and SSS regions, respectively, compared to the 8K experiment (Table 4i).

215 Our analysis shows that this increased vegetation in the 8KCN results from moderated nitrogen limitation on photosynthetic carbon uptake (Eq. (1) and Fig. 7). The nitrogen downregulation fraction defined by GPP/GPP_p is about 0.5 and 0.3 in the NSS and SSS regions, respectively, in the 8K experiment but decreases by about 0.1 in the 8KCN experiment. Our further simulation indicates that vegetation fraction and vegetation types depend on the amount of soil nitrogen (Fig. S3). The increase in vegetation fraction

220 and tree cover fraction are approximately proportional to the amount of soil nitrogen. Vegetation fraction increase is substantially smaller in the 8KCNh (i.e., half nitrogen simulation of the 8KCN) compared to the 8KCN (Fig. S3). Trees in the 8KCN is also substantially replaced by grass and shrub in the simulation with less soil nitrogen (8KCNh).

We speculate that albedo–precipitation feedback is reinforced with more

225 vegetation in the 8KCN experiment. In the 8K experiment, the surface albedo decreases compared to the 0K experiment, mainly because of the increase in soil moisture by the enhanced precipitation. In the 8KCN simulation, the surface albedo diminishes more, because the vegetation increases more, and the surface

230 albedo decreases with increasing vegetation cover. Our further analysis suggests that such feedback reinforcement makes an additional 0.1 mm day^{-1} precipitation and expansion of vegetation, especially in the SSS region (Fig. 8a and 8b).

3.3 Impact of soil texture on the Green Sahara simulation

Soil is classified as sandy soil for the present–day Sahara in the 8K and 8KCN simulations like previous studies on the GS (e.g., Hopcroft et al., 2017; Groner et al., 2018). It is, however, plausible that the

235 soil in the GS includes more nutrients and humus than sandy soil (i.e., loamier) with the extensive vegetations in this humid region because organic matter is formed by decomposition of litter and woody debris (Levis et al., 2004; Koven et al., 2013). Such soil type changes make impacts on soil color as well as soil hydraulic and thermal properties. Compared to sandy soil, loamy soil has larger soil porosity and heat capacity but smaller saturated hydraulic conductivity because they contain more slit and clay than sandy soils.

240 Consequently, loamy soils have larger water-holding (i.e., soil porosity) and heat capacities (Kutzbach et al., 1996; Levis et al., 2004). Previous study based on the offline dynamic vegetation simulation of the GS shows that the simulated greening of the Sahara is sensitive to changes in soil thermal and hydraulic properties without bare-soil albedo changes (Lu et al., 2018).

245 Our fully coupled ESM simulation of 8KCNS ~~corroborates~~also shows that soil texture leads to significant changes in vegetation and climate in North Africa ~~due~~. Vegetation cover fraction shows 78% increase over the SS region when the soil nitrogen and soil texture are modified all together (i.e., 8KCNS experiment), compared to the 8KCN experiment. (Fig. 9e; Table 4). Notably, those feedback processes are critical in the western SSS which is coincident with the region is classified as sandy soil in the ESMs (Fig. 9f–9l). Vegetation fraction increase is clearly observed especially in the western SSS (< 10° E)
250 in the 8KCNS experiment, with a 2° N northward movement (15° N to 17° N) of the 20% vegetation coverage border and its related GPP increases. This result suggests that the western SSS is a hot spot in perspective of soil texture in the EMH simulations.

Our analysis indicate that such substantial sensitivity is mainly related to changes ~~in surface albedo as well as~~ in soil hydraulic and thermal properties.

255 ~~In our 8KCNS simulation, a change from sandy to loamy soil leads to an increase in soil porosity (i.e., water holding capacity) and to~~ but the darker soil color. ~~Accordingly, the higher soil moisture and~~ of loamy soils also regulates climate and vegetation the study region. Relatively darker soil color ~~reduce the~~ of loamy soils in the 8KCNS experiment leads to smaller surface albedo ~~altogether in the 8KCNS simulation~~and its increase in reinforced by increases in summertime precipitation (see Eq. (9); Fig. ~~8a, 8b). These changes lead to an~~9a- 9b). That is, the darker soils enhance absorption of solar radiation (i.e.,
260 increase in surface net radiation,~~).~~ and more available energy is partitioned into latent heat fluxes (i.e., smaller Bowen ratio), leading to more precipitation in ~~the~~ North Africa (Fig. ~~8c 8e)~~9c–9e) possibly through ~~enhanced~~the albedo–precipitation feedback ~~in loamy soils.~~

~~Furthermore, it is worth noting that subsequent increases in evapotranspiration amplifies precipitation by~~ and its related moisture recycling ~~again (e.g., (~~Hopcroft et al., 2017; Levine and Boos, 2017; Groner et al., 2018). ~~Previous~~Also, previous
265 studies ~~have shown~~indicate that ~~the~~enhanced evapotranspiration ~~increase~~results in ~~the Sahara Sahel region made an increase in precipitation~~more rainfall by ~~weaking the~~weakened African Easterly Jet (AEJ) (Cook, 1999; Wu et al., 2009; Rachmayani et al., 2015). Our simulation also reveals that ~~loamy soil and the corresponding vegetation change increases precipitation with enhanced evapotranspiration and weaker AEJ which is not found in the 8KCN experiment. Our results suggest that both the nitrogen fertilization and the soil properties are important to simulate the increases in precipitation and vegetation dynamics.~~
270 ~~Particularly, such feedback processes are dominant in the western SSS where most of this region is classified as sandy soil in the ESMs (Fig. 8f 8l). Indeed, vegetation fraction increase was clearly observed especially in the western SSS (< 10° E) in the 8KCNS experiment, with a 2° N northward movement (15° N to 17° N) of the 20% vegetation coverage border and its related GPP increases. This result suggests that the western SSS is a hot spot in perspective of soil texture in the MH simulations~~AEJ is weakened with more evaporation and summertime rainfall, which is not found in the 8KCN experiment.

4. Summary and conclusion

~~This study aims at exploring the effect of soil nitrogen and soil carbon in an Earth System Model on simulations of the Green Sahara some 8,000 years ago. As we expected,~~The Green Sahara indicates extensive vegetative area and humid climate in the Sahara-Sahel region in the early to mid-Holocene. Previous studies report that the GS is a consequence of complex interactions between various climatic and biophysical factors. It is also known that land-atmosphere interaction enhances vegetation in the GS period with impacts of SST and orbital forcing change (e.g., Claussen et al., 2013; Groner et al., 2018). This study aims at examining the effect of soil nitrogen and soil physical properties on simulations of the Green Sahara 8,000 years ago using the state-of-the-art ESM that incorporates soil nitrogen and albedo-soil moisture feedback processes. As far as we know, this is the first study to investigate impacts of soil nitrogen and soil texture on the GS simulation using the fully coupled ESM.

Our ESM simulation results clearly show that vegetation in the GS is dramatically sensitive to soil organic carbon and soil texture in North Africa (Table 5). With the changes in the Earth's orbit and dust in the EMH, the model simulates the northward movement of the tropical rainfall belt and its related precipitation increases in North Africa ~~are found in the simulations~~ with the ~~8K~~EMH conditions and present–day soil nitrogen and soil carbon. However, despite this more precipitation ~~in this region~~, the meridional extent of vegetation in the Sahara–Sahel transition zone only marginally differs between the early to mid–Holocene and present–day simulation, which did not simulate greening in the early to mid–Holocene properly. This inconsistent modeling behavior between precipitation and vegetation cover can be attributed to the unrealistically high threshold of precipitation required for desert–grassland transition and low WUE in the terrestrial ecosystem model. ~~We show~~Our analysis shows that this excessive rainfall ~~requirement~~need for vegetation is lowered, ~~thus making vegetation cover and GPP increases,~~ if ~~we consider~~ enhanced soil nitrogen and loamier soil are considered in the model based on the extensive vegetation during the ~~Green Sahara period.~~ GS. This change in the vegetation threshold leads to increases in GPP and vegetation cover eventually. Particularly, the SS region is sensitive to soil nitrogen and clay and silt composition in soil (i.e., loamier) in our simulations. Our results suggest that soil property is as important as nitrogen fertilization in simulating precipitation, vegetation dynamics, and atmospheric circulation in North Africa during the EMH.

It is also found that ~~in this soil–nitrogen–enhanced simulation, the~~ the increase in vegetation cover ~~leads to~~ is reinforced by more precipitation in this soil–nitrogen–enhanced simulation through the feedback in soil albedo~~–~~, water holding capacity, soil color, and precipitation~~. Further~~ processes. Our sensitivity simulations show that loamy soil having more soil organic matter also leads to more precipitation and vegetation in the Holocene North Africa through ~~added~~ albedo–precipitation and evapotranspiration–precipitation feedbacks~~.~~ with changes in soil color, soil nitrogen, and soil physical properties. Our results indicate that soil nitrogen through downregulation of GPP and ~~interactive changes in~~process–based dynamics of soil ~~texture~~properties with vegetation are critical for the Green Sahara simulations~~. Notably, our~~ in the ESMs. In particular, GPP and vegetation cover shows dramatic increases of 400% and 150 % in the SS region respectively with changes in soil organic matter and soil texture. Our findings and their implications can be extended to the future climate and dynamic vegetation

서식 있음: 들여쓰기: 첫 줄: 1 글자

simulations ~~and more attention~~. More future study should be paid to the role of soil biogeochemical processes in the vegetation dynamics in climate simulations~~.~~ particularly if we use the ESM to incorporate carbon and nitrogen cycles into the model.

310

Acknowledgements

This research has been supported by the National Research Foundation of Korea grant funded by the South Korean government (MSIT) (grant no. NRF-2018R1A5A1024958) and the Korea Meteorological Administration Research and Development Program under Grant KMI2021-01610.

315

Appendices

A. List of symbols and definitions.

Symbols	Definitions
CF_{alloc}	~~total~~amount of carbon allocated ~~C flux~~to new growth (gC m^{-2} s^{-1})
CF_{avail_allloc}	~~C flux~~amount of total carbon available for new growth allocation (gC m^{-2} s^{-1})
CF_{excess}	~~C flux~~amount of carbon that plants could additionally allocate if nitrogen were not ~~allocated due to downregulation~~limiting (gC m^{-2} s^{-1})
dt	decomposition timestep (seconds)
f_{pg}	fraction of potential ~~GPP~~growth that can be achieved with the nitrogen available to plants (no units)
~~GPP~~GPP_p	gross primary ~~index~~production when there is no nitrogen limitation (gC m^{-2} s^{-1})
k_{c_alloc}/~~k_{n_alloc}~~	~~C~~Carbon:Nitrogen stoichiometry constant for new growth allocation ~~index~~(gC (gN)$^{-1}$)
~~k_{n_alloc}~~	~~N allocation index~~
MR	maintenance respiration (gC m^{-2} s^{-1})
$N_{plant\_ndemand}$	~~plant N~~nitrogen demand by plant for photosynthesis (gN m^{-2} s^{-1})
$N_{retrans}$	~~deployment of retranslocated N (gN m^{-2} s^{-1})~~retranslocated nitrogen pool (gN m^{-2} s^{-1}). Nitrogen retranslocation is the amount of nitrogen that is removed from the tissues and is stored in the other part of the plant to reuse it in the next growth.
N_{sminn}	~~soil~~the amount of mineral ~~N~~nitrogen in the total soil column (gN m^{-2})
N_{uptake}	amount of plant ~~N~~uptake from soil mineral nitrogen pool (gN m^{-2} s^{-1})
NF_{immob}	~~Immobilization N~~amount of immobilized nitrogen flux (gN m^{-2} s^{-1})
$NF_{soil4n \rightarrow sminn}$	nitrogen fluxes leaving soil nitrogen pool with largest turnover time to soil mineral nitrogen (gN m^{-2} s^{-1})
$soil4c$	soil carbon pool with largest turnover time (gC m^{-2})

k_{decomp}	decomposition rate constant of the soil organic matter (no unit)
α_{sat}	soil background albedo for saturated soil (fraction)
α_{soil}	soil background albedo (fraction)
Δ	variable that depends on the volumetric water content of the first soil layer
θ_1	the volumetric soil water content of the first soil layer (m^3 m^{-3})

서식 지정된 표

320 Acknowledgements

This research has been supported by the National Research Foundation of Korea grant funded by the South Korean government (MSIT) (grant no. NRF-2018R1A5A1024958) and the Korea Meteorological Administration Research and Development Program under Grant KMI2021-01610.

References

325 Arora, V. K., Katavouta, A., Williams, R. G., Jones, C. D., Brovkin, V., Friedlingstein, P., Schwinger, J., Bopp, L., Boucher, O., Cadule, P., Chamberlain, M. A., Christian, J. R., Delire, C., Fisher, R. A., Hajima, T., Ilyina, T., Joetzjer, E., Kawamiya, M., Koven, C. D., Krasting, J. P., Law, R. M., Lawrence, D. M., Lenton, A., Lindsay, K., Pongratz, J., Raddatz, T., Séférian, R., Tachiiri, K., Tjiputra, J. F., Wiltshire, A., Wu, T., and Ziehn, T.: Carbon–concentration and carbon–climate feedbacks in CMIP6 models and their comparison to CMIP5 models, Biogeosciences, 17, 4173–4222, https://doi.org/10.5194/bg-17-4173-330 2020, 2020.

Berger, A. L.: Long-Term Variations of Caloric Insolation Resulting from the Earth's Orbital Elements 1, Quat. Res., 9, 139–167, 1978.

Bonfils, C., de Noblet-Ducoudre, N., Braconnot, P., and Joussaume, S.: Hot desert albedo and climate change: Mid-Holocene monsoon in North Africa, J. Climate, 17, 3724–3737, 2001.

335 Braconnot, P., Joussaume, S., Marti, O., and de Noblet, N.: Synergistic Feedbacks from Ocean and Vegetation on the African Monsoon Response to Mid-Holocene Insolation, Geophys. Res. Lett., 26, 2481–2484, 1999.

Braconnot, P., Zhu, D., Marti, O., and Servonnat, J.: Strengths and challenges for transient Mid- to Late Holocene simulations with dynamical vegetation, Clim. Past, 15, 997–1024, https://doi.org/10.5194/cp-15-997-2019, 2019.

Brooks, M. L.: Effects of increased soil nitrogen on the dominance of alien annual plants in the Mojave Desert, J. Appl. Ecol., 340 40, 344-353, 2003.

Broxton, P. D., Zeng, X., Sulla-Menashe, D., and Troch, P. A.: A global land cover climatology using MODIS data, J. Appl. Meteorol. Clim., 53, 1593–1605, doi:10.1175/JAMC-D-13-0270.1, 2014.

Castillo, C. K. G., Levis, S., and Thornton, P. E.: Evaluation of the New CNDV Option of the Community Land Model: Effects of Dynamic Vegetation and Interactive Nitrogen on CLM4 Means and Variability, J. Climate, 25, 3702–3714, 345 doi:10.1175/JCLI-D-11-00372.1, 2012.

Cess, R. D.: Biosphere-Albedo Feedback and Climate Modeling, J. Atmos. Sci., 35, 1765–1768, 1978.

Charney, J. G.: Dynamics of Deserts and Drought in Sahel, Q. J. Roy. Meteor. Soc., 101, 193–202, 1975.

Chikira, M., Abe-Ouchi, A., and Sumi, A.: General circulation model study on the green Sahara during the mid-Holocene: an impact of convection originating above boundary layer, J. Geophys. Res., 111, D21103, doi:10.1029/2005JD006398, 2006.

350 Claussen, M.: On multiple solutions of the atmosphere-vegetation system in present-day climate, Glob. Change Biol., 4, 549–559, 1998.

Claussen, M., Kubatzki, C., Brovkin, V., Ganoposki, A., Hoelzmann, P., and Pachur, H. J.: Simulation of an abrupt change in Saharan vegetation in the mid-Holocene, Geophys. Res. Lett., 26, 2037–2040, 1999.

Claussen, M., Bathiany, S., Brovkin, V., and Kleinen, T.: Simulated climate-vegetation interaction in semi-arid regions
355 affected by plant diversity, Nat. Geosci., 6, 954–958, 2013.

Claussen, M., Dallmeyer, A., and Bader, J.: Theory and modeling of the African humid period and the green Sahara, Oxford Research Encyclopedia of Climate Science, https://doi.org/10.1093/acrefore/9780190228620.013.532, 2017.

Coe, M. and Bonan, G.: Feedbacks between climate and surface water in northern Africa during the middle Holocene, J. Geophys. Res., 102, 11087–11101, doi:10.1029/97JD00343, 1997.

360 Contoux, C., Jost, A., Ramstein, G., Sepulchre, P., Krinner, G., and Schuster, M.: Megalake Chad impact on climate and vegetation during the late Pliocene and the mid-Holocene, Clim. Past, 9, 1417–1430, doi:10.5194/cp-9-1417-2013, 2013.

Gaetani, M., Messori, G., Zhang, Q., Flamant, C., and Pausata, F. S. R.: Understanding the Mechanisms behind the Northward Extension of the West African Monsoon during the Mid-Holocene, J. Climate, 30, 7621–7642, https://doi.org/10.1175/JCLI-D-16-0299.1, 2017.

365 Groner, V. P., Raddatz, T., Reick, C. H., and Claussen, M.: Plant functional diversity affects climate–vegetation interaction, Biogeosciences, 15, 1947–1968, https://doi.org/10.5194/bg-15-1947-2018, 2018.

Harrison, S. P., Bartlein, P. J., Izumi, K., Li, G., Annan, J., Hargreaves, J., Braconnot, P. B., and Kageyama, M.: Implications of evaluation of CMIP5 palaeosimulations for climate projections, Nature Climate Change, 5, 735–743, doi:10.1038/nclimate2649, 2015.

370 Hély, C., Lézine, A.-M., and contributors, A.: Holocene changes in African vegetation: tradeoff between climate and water availability, Clim. Past, 10, 681–686, https://doi.org/10.5194/cp-10-681-2014, 2014.

Hopcroft, P. O., Valdes, P. J., Harper, A. B., and Beerling, D. J.: Multi vegetation model evaluation of the Green Sahara climate regime, Geophys. Res. Lett., 44, 6804–6813, 2017.

Hurrell, J. W., Holland, M. M., Gent, P. R., Ghan, S., Kay, J. E., Kushner, P., Lamarque, J.-F., Large, W. G., Lawrence, D.,
375 Lindsay, K., Lipscomb, W. H., Long, M. C., Mahowald, N., Marsh, D. R., Neale, R. B., Rasch, P., Vavrus, S., Vertenstein, M., Bader, D., Collins, W. D., Hack, J. J., Kiehl, J., and Marshall, S.: The Community Earth System Model: a framework for collaborative research, B. Am. Meteorol. Soc., 94, 1339–1360, 2013.

Houldcroft, C., Grey, W., Barnsley, M., Taylor, C., Los, S., and North, P.: New Vegetation Albedo Parameters and Global Fields of Soil Background Albedo Derived from MODIS for Use in a Climate Model, J. Hydrometeorol., 10(1), 183–198,
380 2009.

Jolly, D., Harrison, S. P., Damnati, B., and Bonnefille, R.: Simulated climate and biomes of Africa during the Late Quaternary: comparisons with pollen and lake status data, Quat. Sci. Rev., 17, 629–657, 1998.

Koven, C.D., Riley, W.J., Subin, Z.M., Tang, J.Y., Torn, M.S., Collins, W.D., Bonan, G.B., Lawrence, D.M. and Swenson, S.C.: The effect of vertically resolved soil biogeochemistry and alternate soil C and N models on C dynamics of
385 CLM4. Biogeosci., *10*(11), 7109-7131, 2013.

Kluzek, E.: CESM research tools: CLM4 in CESM1. 0.4 user's guide documentation, National Centers for Atmospheric Research, Boulder, 2012.

Knorr, W., Schnitzler, K. G., and Govaerts, Y.: The role of bright desert regions in shaping North African climate, Geophys. Res. Lett., 28, 3489–3492, 2001.

390 Knorr, W. and Schnitzler, K. G.: Enhanced albedo feedback in North Africa from possible combined vegetation and soil formation processes, Clim. Dynam., 26, 55–63, 2006.

Krinner, G., Lézine, A. M., Braconnot, P., Sepulchre, P., Ramstein, G., Grenier, C., and Gouttevin, I.: A reassessment of lake and wetland feedbacks on the North African Holocene climate, Geophys. Res. Lett., 39, L07701, doi:10.1029/2012GL050992, 2012.

395 Kutzbach, J. E.: Monsoon climate of the early Holocene: Climate experiment with the Earth's orbital parameters for 9000 years ago, Science, 214, 59–61, 1981.

Kutzbach, J. E. and Street-Perrott, F. A.: Milankovitch forcing of fluctuations in the level of tropical lakes from 18 to 0 kyr BP, Nature, 317, 130–134, 1985.

Kutzbach, J., Bonan, G., Foley, J., and Harrison, S.: Vegetation and soil feedbacks on the response of the African monsoon to 400 orbital forcing in the early to middle Holocene, Nature, 384, 623–626, 1996.

Kutzbach, J. E. and Liu, Z.: Response of the African Monsoon to Orbital Forcing and Ocean Feedbacks in the Middle Holocene, Science, 278. 440–443, 1997.

Larrasoana, J. C., Roberts, A. P., and Rohling, E. J.: Dynamics of Green Sahara periods and their role in Hominin evolution, PLoS ONE, 8, e76514, https://doi.org/10.1371/journal.pone.0076514, 2013.

405 Lawrence, D. M., Oleson, K. W., Flanner, M. G., Thorton, P. E., Swenson, S. C., Lawrence, P. J., Zeng, X., Yang, Z.-L., Levis, S., Skaguchi, K., Bonan, G. B., and Slater, A. G.: Parameterization improvements and functional and structural advances in version 4 of the Community Land Model, J. Adv. Model. Earth Sys., 3, 2011MS000045, doi:10.1029/2011ms000045, 2011.

Leblanc, M., Favreau, G., Maley, J., Nazoumou, Y., Leduc, C., Stagnitti, F., van Oevelen, P. J., Delclaux, F., and Lemoalle, J.: Reconstruction of Megalake Chad using Shuttle Radar Topographic Mission data, Palaeogeogr. Palaeocl., 239, 16–27, 410 doi:10.1016/j.palaeo.2006.01.003, 2006.

Levine, X. J., and W. R. Boos: Land surface albedo bias in climate models and its association with tropical rainfall, Geophys. Res. Lett., 44, 6363-6372. 2017.

Levis, B. S., Bonan, G. B., and Bonfils, C.: Soil feedback drives the mid-Holocene North African monsoon northward in fully coupled CCSM2 simulations with a dynamic vegetation model, Clim. Dynam., 23, 791–802, doi:10.1007/s00382-004-0477-415 y, 2004.

Lu, Z., Miller, P. A., Zhang, Q., Zhang, Q., Wårlind, D., Nieradzik, L., Sjolte, J., and Smith, B.: Dynamic vegetation simulations of the mid-Holocene Green Sahara, Geophys. Res. Lett., 45, 8294-8303, 2018.

Neale, R. B., Richter, J., Park, S., Lauritzen, P. H., Vavrus, S. J., Rasch, P. J., and Zhang, M.: The Mean Climate of the Community Atmosphere Model (CAM4) in Forced SST and Fully Coupled Experiments, J. Climate, 26, 5150–5168, doi:10.1175/JCLID-12-00236.1, 2013.

420

Oleson, K. W., Lawrence, D. M., Bonan, G. B., Flanner, M. G., Kluzek, E., Lawrence, P. J., Levis, S., Swenson, S. C., Thornton, P. E., Dai, A., Decker, M., Dickinson, R., Feddema, J., Heald, C. L., Hoffman, F., Lamarque, J.-F., Mahowald, N., Niu, G.-Y., Qian, T., Randerson, J., Running, S., Sakaguchi, K., Slater, A., Stockli, R., Wang, A., Yang, Z.-L., Zeng, X., and Zeng, X.: Technical Description of version 4.0 of the Community Land Model (CLM), Tech. Rep. NCAR/TN-478+STR, National Center

425
for Atmospheric Research, Boulder, Colorado, USA, 2010.

Pausata, F. S. R., Messori, G., and Zhang, Q.: Impacts of dust reduction on the northward expansion of the African monsoon during the Green Sahara period, Earth Planet. Sc. Lett., 434, 298–307, 2016.

Pausata, F. S., Gaetani, M., Messori, G., Berg, A., de Souza, D. M., Sage, R. F., and deMenocal, P. B.: The Greening of the Sahara: Past Changes and Future Implications, One Earth, 2, 235–250, 2020.

430
Quade, J., Dente, E., Armon, M., Dor, Y. B., Morin, E., Adam, O., and Enzel, Y.: Megalakes in the Sahara? A review, Quat. Res., 90, 253-275, 2018.

Rachmayani, R., Prange, M., and Schulz, M.: North African vegetation-precipitation feedback in early and mid-Holocene climate simulations with CCSM3-DGVM, Clim. Past, 11, 175–185, doi:10.5194/cp-11-175-2015, 2015.

Schuster, M., Roquin, C., Duringer, P., Brunet, M., Caugy, M., Fontugne, M., Mackaye, H. T., Vignaud, P., and Ghienne, J.

435
F.: Holocene Lake Mega-Chad palaeoshorelines from space, Quatern. Sci. Rev., 24, 1821–1827, 2005.

Shanahan, T. M., McKay, N. P., Hughen, K. A., Overpeck, J. T., Otto-Bliesner, B., Heil, C. W., King, J., Scholz, C. A., and Peck, J.: The time-transgressive termination of the African Humid Period, Nat. Geosci., 8, 140–144, https://doi.org/10.1038/ngeo2329, 2015.

Stringer, L. C., Akhtar-Schuster, M., Marques, M. J., Amiraslani, F., Quatrini, S., and Abraham, E. M.: Combating land

440
degradation and desertification and enhancing food security: Towards integrated solutions, Ann. Arid Zone, 50, 1-23, 2012.

Takata, K., Emori, S., and Watanabe, T.: Development of the minimal advanced treatments of surface interaction and runoff, Global Planet. Change, 38, 209–222, doi:10.1016/S0921- 8181(03)00030-4, 2003.

Thornton, P. E., Law, B. E., Gholz, H. L., Clark, K. L., Falge, E., Ellsworth, D. S., Goldstein, A. H., Monson, R. K., Hollinger, D., Falk, M., Chen, J., and Sparks, J. P.: Modeling and measuring the effects of disturbance history and climate on carbon and

445
water budgets in evergreen needleleaf forests, Agr. Forest Meteorol., 113, 185–222, doi:10.1016/S0168-1923(02)00108-9, 2002.

Thornton, P. and Rosenbloom, N.: Ecosystem model spin-up: Estimating steady state conditions in a coupled terrestrial carbon and nitrogen cycle model, Ecol. Model., 189, 25–48, doi:10.1016/j.ecolmodel.2005.04.008, 2005.

Thornton, P. E., Lamarque, J.-F., Rosenbloom, N. A., and Mahowald, N. M.: Influence of carbon-nitrogen cycle coupling on

450
land model response to CO2 fertilization and climate variability, Global Biogeochem. Cy., 21, doi:10.1029/2006GB002868, 2007.

Thornton, P. E., Doney, S. C., Lindsay, K., Moore, J. K., Mahowald, N., Randerson, J. T., Fung, I., Lamarque, J.-F., Feddema, J. J., and Lee, Y.-H.: Carbon-nitrogen interactions regulate climate-carbon cycle feedbacks: results from an atmosphere-ocean general circulation model, Biogeosciences, 6, 2099–2120, doi:10.5194/bg-6-2099-2009, 2009.

455 Tierney, J. E., Pausata, F. S., and deMenocal, P. B.: Rainfall regimes of the Green Sahara, Sci. Adv., 3, e1601503, https://doi.org/10.1126/sciadv.1601503, 2017.

Vamborg, F. S. E., Brovkin, V., and Claussen, M.: The effect of a dynamic background albedo scheme on Sahel/Sahara precipitation during the mid-Holocene, Clim. Past, 7, 117–131, doi:10.5194/cp-7-117-2011, 2011.

Wang, Y., Li, Y., Ye, X., Chu, Y., and Wang, X.: Profile storage of organic/inorganic carbon in soil: From forest to desert, 460 Sci. Total Environ., 408, 1925–1931, doi:10.1016/j.scitotenv.2010.01.015, 2010.

Watanabe, M., Suzuki, T., O'ishi, R., Komuro, Y., Watanabe, S., Emori, S., Takemura, T., Chikira, M., Ogura, T., Sekiguchi, M., Takata, K., Yamazaki, D., Yokohata, T., Nozawa, T., Hasumi, H., Tatebe, H., and Kimoto, M.: Improved Climate Simulation by MIROC5: Mean States, Variability, and Climate Sensitivity, J. Climate, 23, 6312–6335, doi:10.1175/2010JCLI3679.1, 2010.

465 Wu, M. L. C., Reale, O., Schubert, S. D., Suarez, M. J., Koster, R. D., and Pegion, P. J.: African easterly jet: Structure and maintenance, J. Climate, 22, 4459–4480, https://doi.org/10.1175/2009JCLI2584.1, 2009.

Yang, R., Su, Y., Wang, M., Wang, T., Yang, X., Fan, G., and Wu, T.: Spatial pattern of soil organic carbon in desert grasslands of the diluvial-alluvial plains of northern Qilian Mountains, Journal of Arid Land, 6, 136–144, 2014.

Zeng, X.: Overview of soil, vegetation, and snow albedos in weather and climate models, Annual meeting of the American 470 Meteorological Society, 79, 81-94, 2005.

Table 1: The abbreviations of the numerical experiments conducted in this study.

Abbreviation	Description
0K	500 years simulation using the pre–industrial conditions for orbital forcing and CO_2 concentration (284.725 ppm).
8K	500 years simulation using the early to mid–Holocene conditions for orbital forcing and CO_2 concentration (Table 2).
8KCN	Same as 8K except that soil carbon and nitrogen are prescribed as the values in the current Sahel region.
8KCN0L	Same as 8KCN except that the Mega Lake Mega Chad is not considered in the simulation.
8KCNh	Same as 8KCN except that soil carbon and nitrogen are prescribed as half of the 8KCN simulation.
8KCNS	Same as 8KCN except that the North African soil was precribed as loam.

475

Table 2: Orbital parameters prescribed for the simulations.

Simulation	CO_2 concentration	Eccentricity	Obliquity	Longitude of Perihelion
0K	284.725 ppm	0.016704	23.44	283.01°
8K, 8KCN, 8KCN0L,8KCNh, 8KCNS	259.9 ppm	0.019101	24.209	148.58°

Table 3: 20% vegetation coverage transition rainfall for OBS (Observation data) and 4 model simulations (the Joint UK Land Environment
480 Simulator version 4.1, Lund-Potsdam-Jena dynamic vegetation model version 2.1, Sheffield Dynamic Global Vegetation Model, and CLM4
for this study). OBS and JULES, LPJ, SDGVM indicates the value from the observation and model simulation in the pre–industrial conditions
which is from Hopcroft et al., 2017.

Model name	20% vegetation coverage transition rainfall (mm yr^{-1})
SDGVM	182
OBS	281
JULES	378
LPJ	515
This study	570 (0K)
	577 (8K)
	412 (8KCN)

485 ~~Table 4~~Table 4: Vegetation fraction (%) and GPP (gC m^{-2} $month^{-1}$) in the SS region. Values in parenthesis are percentage changes in vegetation fraction and GPP to the 0K simulation.

	0K	8K	8KCN	8KCNS
Vegetation fraction (percentage change in vegetation fraction to the 0K simulation)	8.3 (0%)	8.3	15.0 (81%)	20.9 (152%)
GPP (percentage change in GPP to the 0K simulation)	3.0 (20%)	2.5	10.3 (312%)	12.6 (404%)

Table 5: GPP (gC m^{-2} month^{-1}) from 5 CMIP5 models (IPSL-CM5A-LR, MIROC-ESM, bcc-csm1-1, MPI-ESM-P, CCSM4) and this study in NSS region (18–22 °N) during the pre–industrial period (PI) and early to mid–Holocene (MHEMH).

Model name	PI GPP	MHEMH GPP
IPSL-CM5A-LR	0.00	0.01
MIROC-ESM	0.06	2.69
CCSM4	0.13	0.50
bcc-csm1-1	1.47	1.65
MPI-ESM-P	1.62	5.21
This study	2.12 (0K)	2.27 (8K) 6.79 (8KCN) 6.82 (8KCNS)
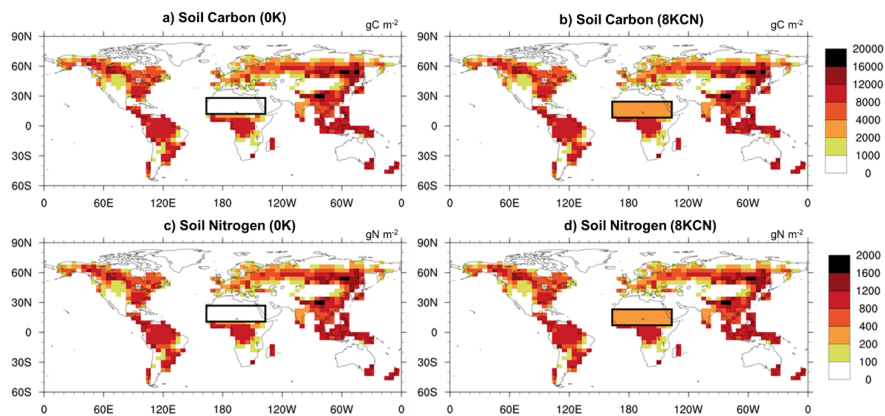
495   Figure 1: Global maps of soil carbon and nitrogen used in the 0K and 8KCN simulations. Values in boxed area is modified in the 8KCN experiment.
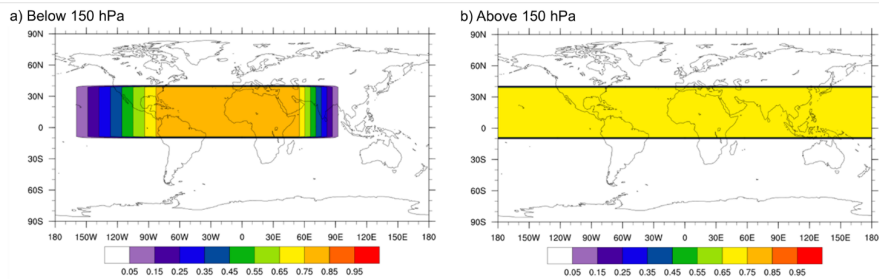
500   Figure 2: Dust reduction fraction a) below 150 hPa and b) above 150 hPa in the early to mid–Holocene experiments compared to the present–day values.
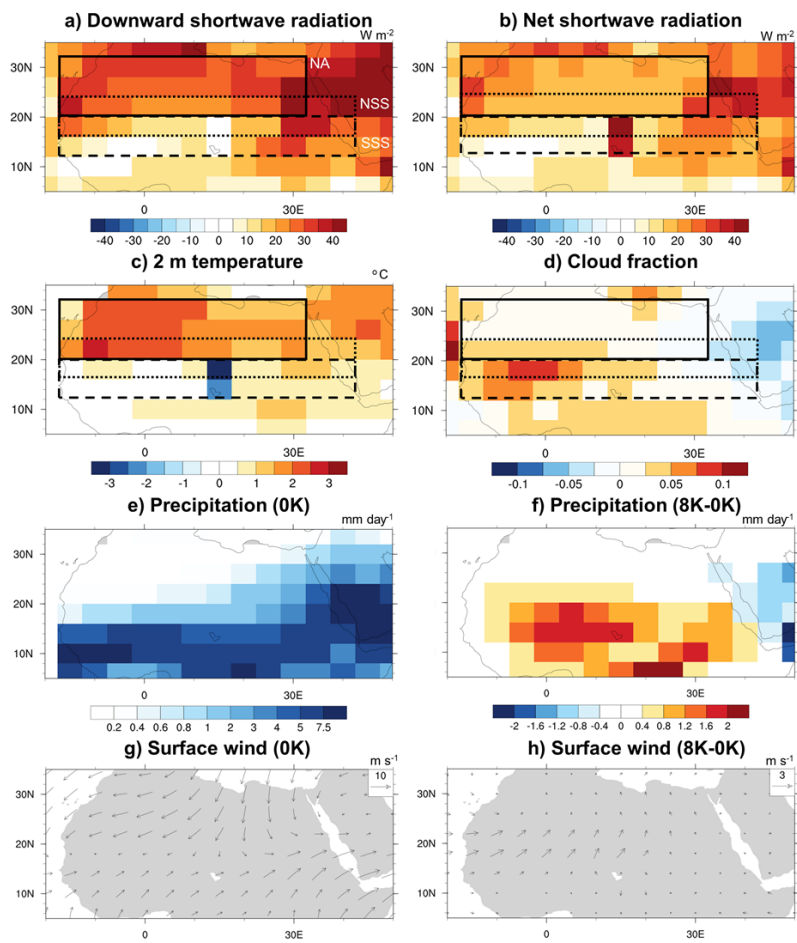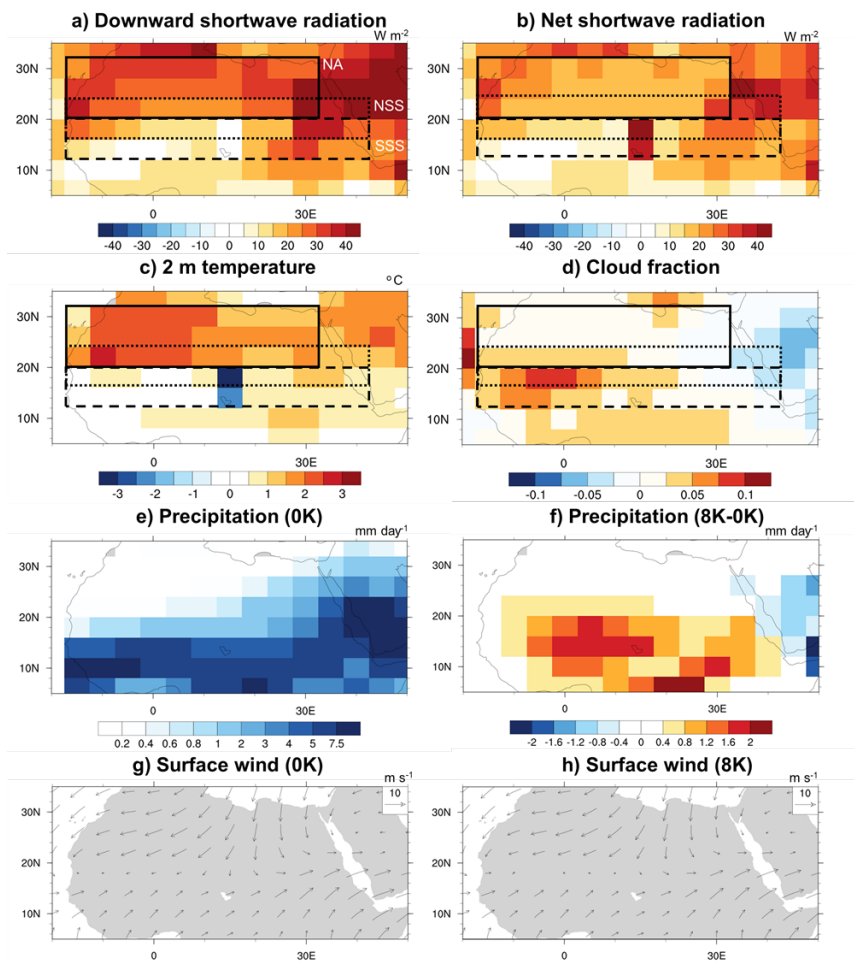
505   Figure 3: Differences of climate conditions between the 8K and 0K experiment (8K-0K) in summer (June, July, August, and September; JJAS). Differences in downward shortwave radiation (a), surface net shortwave radiation (b), 2 m air temperature (c), and cloud fraction (d). (e) and (f) are JJAS precipitation in the 0K and its differences from the 8K experiment and (g) and (f)h) are JJAS surface wind vector of 0K and ~~its differences from the~~ 8K experiment respectively. Black squared boxes are the NA (solid), NSS (dotted), SSS (dashed) areas.

510
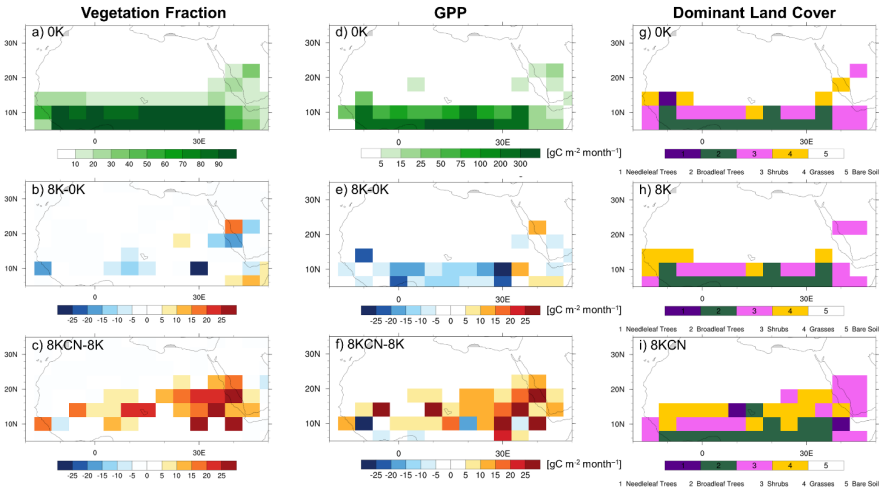
Figure 4: Vegetation fraction (left column), summertime GPP (middle column), and dominant land cover (right column). Panels (b), (e) and (c), (f) are differences between 8K and 0K and between 8KCN and 8K, respectively. Dominant land cover is decided as bare soil if vegetation cover fraction is less than 20%.

515
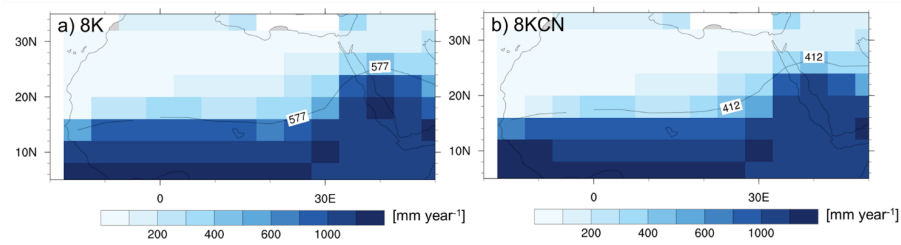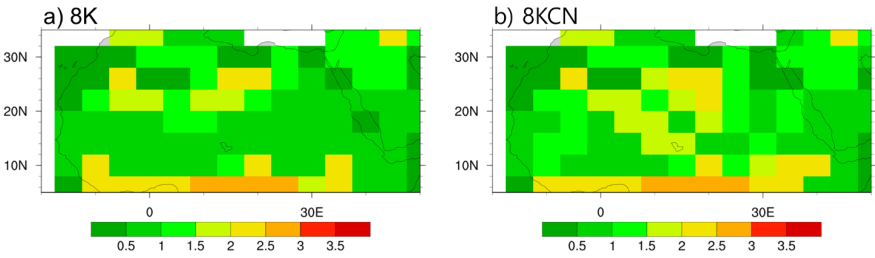
Figure 5

Figure 5: WUE (Water Use Efficiency) during the growing season in the 8K (a) and 8KCN (b) simulations.

520
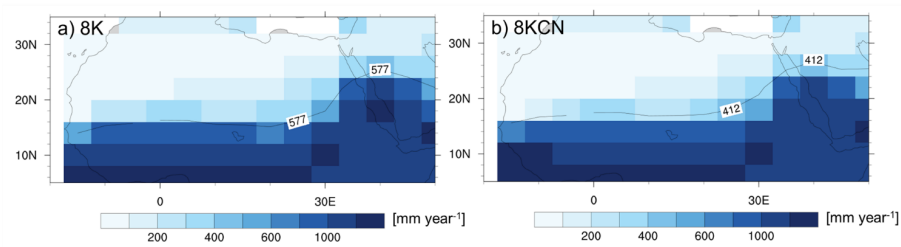
525 Figure 6: Annual precipitation in North African from a) the 8K b) 8KCN simulations. The minimum amount of precipitation for vegetation growth boundary is plotted as a black line with its values.
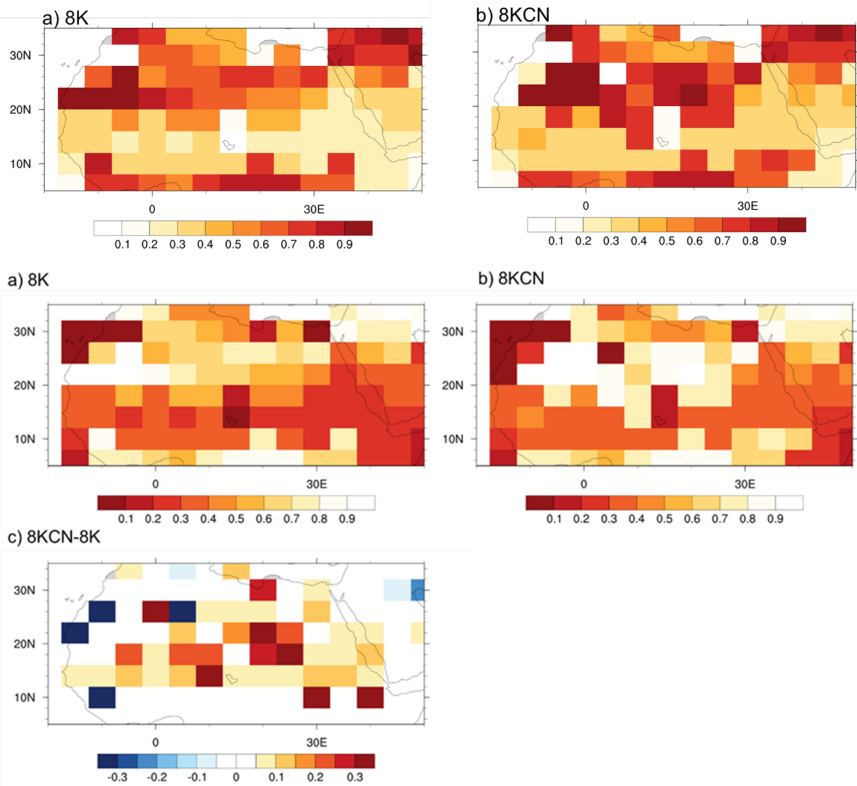
Figure 67: Downregulation fraction (GPP divided by GPP not limited by nitrogen) in the a) 8K and b) 8KCN simulations. (top). Downregulation fraction difference between in the 8KCN and 8K simulation (bottom, Figure 7c).
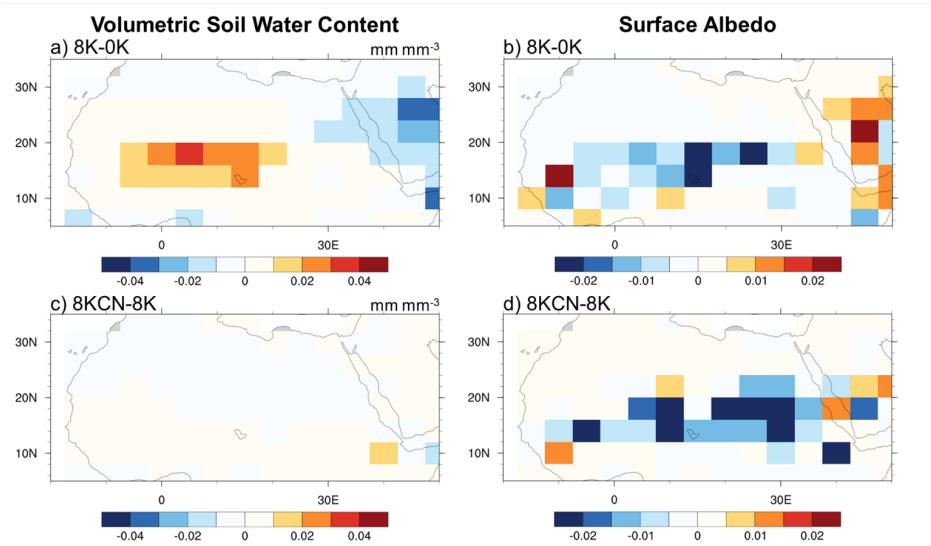
Figure 78: Differences in volumetric soil water content (left) and surface albedo (right) between the 0K, 8K, and 8KCN experiments. The first and second rows show the differences between the 8K and 0K, between the 8KCN and 8Kexperiments, respectively.
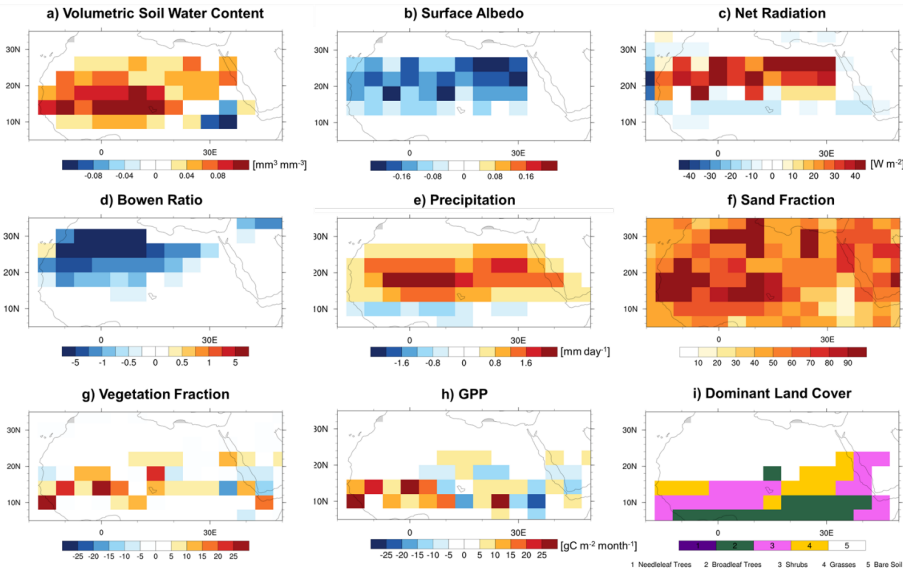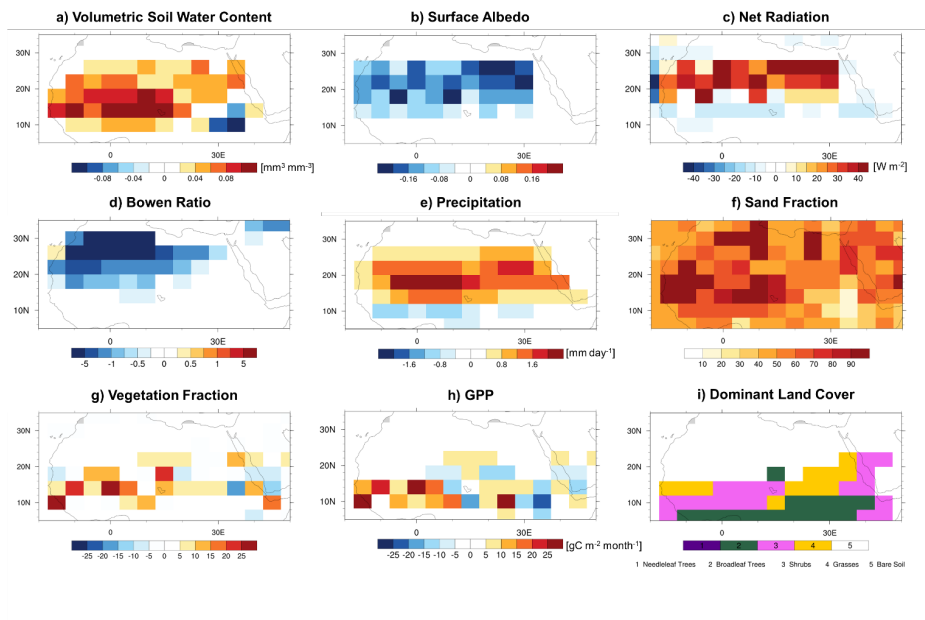
Figure 89: Differences of the loamy soil experiment (8KCNS) from 8KCN. (a) volumetric soil water content, (b) surface albedo, (c) net shortwave radiation, (d) Bowen ratio, (e) precipitation, (f) default sand fraction in grid used in 8K and 8KCN, (g) evapotranspiration, (h) 600 hPa wind of 8KCN, (i) 600 hPa wind difference, (j) vegetation fraction, (k) GPP, and (l) dominant land cover in the 8KCNS experiment. Only grids that are significantly different at 95% in a Student's t test are colored in Figure 9e. Soil type is decided as the relative percentages of sand, silt and clay in soil and soil physical parameters are assigned based on this soil type in the CLM model (Figure 8f; Bonan et al., 2002).

페이지 4: [1] 서식 지정함 Jinkyu Hong 2021. 12. 8. AM 10:27:00

글꼴 색: 텍스트 1

페이지 4: [1] 서식 지정함 Jinkyu Hong 2021. 12. 8. AM 10:27:00

글꼴 색: 텍스트 1

페이지 4: [1] 서식 지정함 Jinkyu Hong 2021. 12. 8. AM 10:27:00

글꼴 색: 텍스트 1

페이지 4: [1] 서식 지정함 Jinkyu Hong 2021. 12. 8. AM 10:27:00

글꼴 색: 텍스트 1

페이지 4: [1] 서식 지정함 Jinkyu Hong 2021. 12. 8. AM 10:27:00

글꼴 색: 텍스트 1

페이지 4: [2] 서식 지정함 Jinkyu Hong 2021. 12. 8. AM 10:27:00

글꼴 색: 텍스트 1

페이지 4: [2] 서식 지정함 Jinkyu Hong 2021. 12. 8. AM 10:27:00

글꼴 색: 텍스트 1

페이지 4: [2] 서식 지정함 Jinkyu Hong 2021. 12. 8. AM 10:27:00

글꼴 색: 텍스트 1

페이지 4: [2] 서식 지정함 Jinkyu Hong 2021. 12. 8. AM 10:27:00

글꼴 색: 텍스트 1

페이지 4: [2] 서식 지정함 Jinkyu Hong 2021. 12. 8. AM 10:27:00

글꼴 색: 텍스트 1

페이지 4: [2] 서식 지정함 Jinkyu Hong 2021. 12. 8. AM 10:27:00

글꼴 색: 텍스트 1

페이지 4: [2] 서식 지정함 Jinkyu Hong 2021. 12. 8. AM 10:27:00

글꼴 색: 텍스트 1

글꼴 색: 텍스트 1

페이지 4: [3] 서식 지정함   **Jinkyu Hong**   **2021. 12. 8. AM 10:27:00**

글꼴 색: 텍스트 1

페이지 4: [3] 서식 지정함   **Jinkyu Hong**   **2021. 12. 8. AM 10:27:00**

글꼴 색: 텍스트 1

페이지 4: [3] 서식 지정함   **Jinkyu Hong**   **2021. 12. 8. AM 10:27:00**

글꼴 색: 텍스트 1

페이지 4: [4] 서식 지정함   **Jinkyu Hong**   **2021. 12. 8. AM 10:27:00**

글꼴 색: 텍스트 1

페이지 4: [4] 서식 지정함   **Jinkyu Hong**   **2021. 12. 8. AM 10:27:00**

글꼴 색: 텍스트 1

페이지 4: [4] 서식 지정함   **Jinkyu Hong**   **2021. 12. 8. AM 10:27:00**

글꼴 색: 텍스트 1

페이지 4: [4] 서식 지정함   **Jinkyu Hong**   **2021. 12. 8. AM 10:27:00**

글꼴 색: 텍스트 1

페이지 4: [4] 서식 지정함   **Jinkyu Hong**   **2021. 12. 8. AM 10:27:00**

글꼴 색: 텍스트 1

페이지 4: [5] 서식 지정함   **Jinkyu Hong**   **2021. 12. 8. AM 10:27:00**

글꼴 색: 텍스트 1

페이지 4: [5] 서식 지정함   **Jinkyu Hong**   **2021. 12. 8. AM 10:27:00**

글꼴 색: 텍스트 1

페이지 4: [5] 서식 지정함   **Jinkyu Hong**   **2021. 12. 8. AM 10:27:00**

글꼴 색: 텍스트 1

페이지 4: [6] 서식 지정함   **Jinkyu Hong**   **2021. 12. 8. AM 10:27:00**

글꼴 색: 텍스트 1

페이지 4: [6] 서식 지정함   **Jinkyu Hong**   **2021. 12. 8. AM 10:27:00**

글꼴 색: 텍스트 1

페이지 4: [6] 서식 지정함   **Jinkyu Hong**   **2021. 12. 8. AM 10:27:00**

글꼴 색: 텍스트 1

페이지 4: [6] 서식 지정함   **Jinkyu Hong**   **2021. 12. 8. AM 10:27:00**

글꼴 색: 텍스트 1

페이지 4: [7] 서식 지정함   **Jinkyu Hong**   **2021. 12. 8. AM 10:27:00**

글꼴 색: 텍스트 1

페이지 4: [7] 서식 지정함   **Jinkyu Hong**   **2021. 12. 8. AM 10:27:00**

글꼴 색: 텍스트 1

페이지 4: [7] 서식 지정함   **Jinkyu Hong**   **2021. 12. 8. AM 10:27:00**

글꼴 색: 텍스트 1

페이지 4: [7] 서식 지정함   **Jinkyu Hong**   **2021. 12. 8. AM 10:27:00**

글꼴 색: 텍스트 1

페이지 4: [7] 서식 지정함   **Jinkyu Hong**   **2021. 12. 8. AM 10:27:00**

글꼴 색: 텍스트 1